

---

# Physics Regularized Gaussian Processes

---

Zheng Wang, Wei Xing, Robert Kirby, Shandian Zhe

School of Computing, University of Utah  
Salt Lake City, UT 84112

wzhut@cs.utah.edu, wxing@sci.utah.edu, kirby@cs.utah.edu, zhe@cs.utah.edu

## Abstract

We consider incorporating incomplete physics knowledge, expressed as differential equations with latent functions, into Gaussian processes (GPs) to improve their performance, especially for limited data and extrapolation. While existing works have successfully encoded such knowledge via kernel convolution, they only apply to linear equations with analytical Green's functions. The convolution can further restrict us from fusing physics with highly expressive kernels, *e.g.*, deep kernels. To overcome these limitations, we propose Physics Regularized Gaussian Process (PRGP) that can incorporate both linear and nonlinear equations, does not rely on Green's functions, and is free to use arbitrary kernels. Specifically, we integrate the standard GP with a generative model to encode the differential equation in a principled Bayesian hybrid framework. For efficient and effective inference, we marginalize out the latent variables and derive a simplified model evidence lower bound (ELBO), based on which we develop a stochastic collapsed inference algorithm. Our ELBO can be viewed as a posterior regularization objective. We show the advantage of our approach in both simulation and real-world applications.

## 1 Introduction

Gaussian processes (GPs) are powerful nonparametric function estimators. However, as a data-driven approach, GPs can perform poorly when the training data are insufficient to reflect the complexity of the system (producing the data) or the test points are far away from the training examples, *i.e.*, extrapolation. On the other hand, physics knowledge, expressed as differential equations, are used

to build physical models for various science and engineering applications (Lapidus and Pinder, 2011). These models are meant to characterize the underlying mechanism (*i.e.*, physical processes) that drives the system and are much less restricted by data availability: they can make accurate predictions even without training data, *e.g.*, the landing of Curiosity on Mars and flight of Voyager 1.

Therefore, we consider improving GP learning with physics knowledge, especially for scarce data and extrapolation tasks. However, encoding physics into a probabilistic framework is challenging. First, differential equations are hard to represent as a probabilistic term, *e.g.*, priors and likelihoods. Second, physics knowledge are usually incomplete — the equations can include latent functions (or sources), making their representations and joint estimation with GPs even more challenging.

While the classical latent force models (LFM) Alvarez et al. (2009, 2013) can incorporate physics by kernel convolution, they are restricted to linear equations with analytical Green's functions to enable the convolution operation. However, many realistic/complex equations are nonlinear and (or linear but) do not have analytical Green's functions, hence cannot be exploited. Furthermore, to obtain a closed-form kernel, we have to convolve with simple/smooth kernels (*e.g.*, Gaussian), which restrict us from fusing physics with complex yet highly expressive kernels, *e.g.*, deep kernels (Wilson et al., 2016), unless we develop extra approximations.

To address these issues, we propose PRGP, a physics regularized GP model to avoid relying on Green's functions, exploit both linear and nonlinear differential equations, and be free to use all kinds of expressive kernels. Specifically, we integrate the standard GP with a generative model in a principled Bayesian hybrid framework (Lasserre et al., 2006). The generative component samples virtual observations and is equivalent to giving a GP prior to the latent function (source) in the equation. We then apply the differential operator (of the equation)

on the posterior function of the standard GP and construct a Dirac delta prior to tightly link to the latent function in the generative component. In this way, we incorporate the information of the equation, without the need for limiting the kernel and equation types. For efficient and good-quality inference, we marginalize out all the latent variables to avoid approximating their complex posteriors. Then we use Jensen’s inequality to derive a simplified model evidence lower bound (ELBO), based on which we develop a stochastic collapsed inference algorithm. The ELBO can be further explained as a soft posterior regularization objective (Ganchev et al., 2010), regularized by physics.

For evaluation, we examined PRGP in both simulations and real-world applications. PRGP uses a shallow kernel for the latent function as in LFM, and a deep kernel for the standard GP component, while LFM convolves the shallow kernel with Green’s function to derive the final kernel for GP estimation. On synthetic datasets based on two commonly used differential equations, PRGP outperforms the standard deep kernel GP, shallow kernel GP and LFM in recovering the ground-truth functions, especially in extrapolation. We then examined PRGP in four real-world applications. PRGP consistently improves upon the competing approaches in prediction accuracy. In addition, we applied PRGP for a nonlinear differential equation where LFM is unavailable. PRGP significantly outperforms standard GPs with deep/shallow kernels.

## 2 Background

**Standard Gaussian Process.** Suppose we aim to learn a function  $f : \mathbb{R}^d \rightarrow \mathbb{R}$  from a training set  $\mathcal{D} = (\mathbf{X}, \mathbf{y})$ , where  $\mathbf{X} = [\mathbf{x}_1, \dots, \mathbf{x}_N]^\top$ ,  $\mathbf{y} = [y_1, \dots, y_N]^\top$ , each  $\mathbf{x}_n$  is a  $d$  dimensional input vector and  $y_n$  the observed output. We place a GP prior,  $f \sim \mathcal{GP}(m(\cdot), k(\cdot, \cdot))$  where  $m(\cdot)$  is the mean function usually set to constant 0 and  $k(\cdot, \cdot)$  the covariance (kernel) function. Then, the finite projection of  $f(\cdot)$  on  $\mathbf{X}$ , namely  $\mathbf{f} = [f(\mathbf{x}_1), \dots, f(\mathbf{x}_N)]^\top$ , follow a multivariate Gaussian distribution,  $p(\mathbf{f}|\mathbf{X}) = \mathcal{N}(\mathbf{f}|\mathbf{0}, \mathbf{K})$  where  $\mathbf{K}$  is the kernel matrix on  $\mathbf{X}$  and each  $[\mathbf{K}]_{i,j} = k(\mathbf{x}_i, \mathbf{x}_j)$ . Given the function values  $\mathbf{f}$ , the observed outputs  $\mathbf{y}$  are sampled from a noisy model. For example, when  $\mathbf{y}$  are continuous, we can use the isotropic Gaussian noise model,  $p(\mathbf{y}|\mathbf{f}) = \mathcal{N}(\mathbf{y}|\mathbf{f}, \tau^{-1}\mathbf{I})$  where  $\tau$  is the inverse variance. We integrate out  $\mathbf{f}$  to obtain the marginal likelihood,

$$p(\mathbf{y}|\mathbf{X}) = \mathcal{N}(\mathbf{y}|\mathbf{0}, \mathbf{K} + \tau^{-1}\mathbf{I}). \quad (1)$$

To learn the model, we can maximize the likelihood to estimate the kernel parameters and the inverse variance  $\tau$ . Given a test input  $\mathbf{x}^*$ , we use a conditional Gaussian distribution to represent the posterior (or predictive) dis-

tribution of  $f(\mathbf{x}^*)$ ,

$$p(f(\mathbf{x}^*)|\mathbf{x}^*, \mathbf{X}, \mathbf{y}) = \mathcal{N}(f(\mathbf{x}^*)|\mu(\mathbf{x}^*), v(\mathbf{x}^*)), \quad (2)$$

where  $\mu(\mathbf{x}^*) = \mathbf{k}_*^\top(\mathbf{K} + \tau^{-1}\mathbf{I})^{-1}\mathbf{y}$ ,  $v(\mathbf{x}^*) = k(\mathbf{x}^*, \mathbf{x}^*) - \mathbf{k}_*^\top(\mathbf{K} + \tau^{-1}\mathbf{I})^{-1}\mathbf{k}_*$  and  $\mathbf{k}_* = [k(\mathbf{x}^*, \mathbf{x}_1), \dots, k(\mathbf{x}^*, \mathbf{x}_N)]^\top$ .

**Latent Force Model.** In many applications, physics knowledge, expressed as differential equations, provides the insight of the system mechanism and can be very useful for prediction. The latent force model (LFM) (Alvarez et al., 2009, 2013) is the classical and state-of-the-art approach to incorporate the physics knowledge into GP learning. In general, LFM considers  $Q$  output functions  $\{f_1(\mathbf{x}), \dots, f_Q(\mathbf{x})\}$ , and assumes each output function  $f_q(\mathbf{x})$  is governed by a linear differential equation,

$$Lf_q(\mathbf{x}) = u_q(\mathbf{x}) \quad (3)$$

where  $L$  is the linear differential operator (Courant and Hilbert, 2008),  $u_q$  a latent function (force) that can be further decomposed as a linear combination of several common latent functions (forces),  $u_q(\mathbf{x}) = \sum_{r=1}^R s_{rq}g_r(\mathbf{x})$ . Since  $L$  is linear, if we assign a GP prior over  $u_q$ ,  $f_q(\mathbf{x})$  will also have a GP prior. Further, if Green’s function (Arfken et al., 2011) — the solution of  $LG(\mathbf{x}, \mathbf{s}) = \delta(\mathbf{s} - \mathbf{x})$  ( $\delta$  is the Dirac delta function) — is available, we can obtain  $f_q(\mathbf{x}) = \int G(\mathbf{x}, \mathbf{s})u_q(\mathbf{s})d\mathbf{s}$ . Hence, given the GP kernel for  $u_q$ , we can derive the kernel for  $f_q$  through a convolution operation,  $k_{f_q}(\mathbf{x}_1, \mathbf{x}_2) = \iint G(\mathbf{x}_1, \mathbf{s}_1)G(\mathbf{x}_2, \mathbf{s}_2)k_{u_q}(\mathbf{s}_1, \mathbf{s}_2)d\mathbf{s}_1d\mathbf{s}_2$ . To handle multiple outputs, we can place (independent) GP priors over each common latent function  $g_r$ , then each  $u_q$  and  $f_q$  will in turn obtain GP priors. Via a similar convolution, we can derive the kernel across different outputs,  $k_{f_q, f_{q'}}(\cdot, \cdot)$ . In this way, the physics knowledge (reflected in Green’s functions) are fused with the kernel for the latent forces, resulting in an convolved kernel, with which we can train the GP model.

## 3 Model

Despite the success of LFM, the precondition for using LFM might be too restrictive. To enable the kernel convolution, LFM requires that the differential equations must be linear and have analytical Green’s functions. However, many realistic/complex equations can be nonlinear (e.g., Burger’s equation (Olsen-Kettle, 2011)) and (or linear but) do not possess analytical Green’s functions; hence they cannot be exploited. In particular cases, even with a tractable Green’s function, a complete kernel of all the input variables is still infeasible to obtain. For example, the Green’s function of the commonly used diffusion equation (Olsen-Kettle, 2011) takes the form  $G(x, \xi, t)$  ( $x$  and  $t$  are spatial and time variables) (Polyanin and Nazaikin-

skaa, 2015), with which we can only convolve on  $\xi$  to obtain a kernel of spatial variables (at a fixed time  $t$ ), and we cannot incorporate different time variables. Finally, in order to obtain an analytical kernel after the convolution, we have to convolve Green’s functions with simple/smooth kernels (*e.g.*, Gaussian). This may prevent us from integrating the physics knowledge into more complex yet highly flexible kernels. For example, the recently proposed deep kernels (Wilson et al., 2016) are constructed from deep neural networks, can perform much better feature mapping than the shallow ones and greatly improve the performance. To handle the intractable integral, we need to develop extra approximations, *e.g.*, Monte-Carlo approximation.

To address these issues, we propose PRGP, a physics regularized GP model that does not count on Green’s functions, can exploit both linear and nonlinear equations, and is free to use all kinds of expressive kernels. Our model is presented as follows.

### 3.1 Physics Regularized Gaussian Process

First, we assume the differential equation that describes the physics knowledge in general takes the following form,

$$\psi f(\mathbf{x}) = g(\mathbf{x}) \quad (4)$$

where  $\psi$  is a differential operator, linear or nonlinear,  $f(\mathbf{x})$  is the target function we want to estimate from a training dataset  $\mathcal{D} = (\mathbf{X}, \mathbf{y})$ ,  $g(\mathbf{x})$  is a latent function (or force) and we do not know its form. Note that the operator  $\psi$  may include unknown parameters as well. One example is  $\psi f(x) = \frac{df(x)}{dx} + \alpha f(x) - \beta$ , where  $\alpha$  and  $\beta$  are unknown parameters. This is a linear operator and the input variable  $x$  is a scalar. Another example is the viscous version of Burger’s equation (Olsen-Kettle, 2011),  $\psi f(\mathbf{x}) = \frac{\partial f(\mathbf{x})}{\partial x_1} + f(\mathbf{x}) \frac{\partial f(\mathbf{x})}{\partial x_2} - v \frac{\partial^2 f(\mathbf{x})}{\partial x_2^2}$ , where  $\mathbf{x} = [x_1, x_2]^\top$ ,  $x_1$  is the spatial variable,  $x_2$  the time variable, and  $v$  the unknown viscosity parameter. This is a nonlinear equation (due to the product term  $f(\mathbf{x}) \frac{\partial f(\mathbf{x})}{\partial x_2}$ ) and does not have any analytical Green’s function. To incorporate the physics knowledge in (4), we propose a hybrid of conditional and generative models based on the general framework proposed by Lasserre et al. (2006). The conditional component is the standard GP that given the training inputs  $\mathbf{X}$ , samples the (noisy) output observations  $\mathbf{y}$ , and the probability  $p(\mathbf{y}|\mathbf{X})$  is provided in (1). To benefit learning, we can choose any expressive kernel (covariance) function, like deep kernels. The generative component is for the unknown function (source)  $g(\mathbf{x})$  in (4). As in LFM, we want to assign a GP prior over  $g(\cdot)$ . To this end, we first sample a finite set of input locations  $\mathbf{Z} = [\mathbf{z}_1, \dots, \mathbf{z}_m]^\top$  (we will discuss the choice of  $p(\mathbf{Z})$  later). Then the projection of  $g$  on  $\mathbf{Z}$  follows a

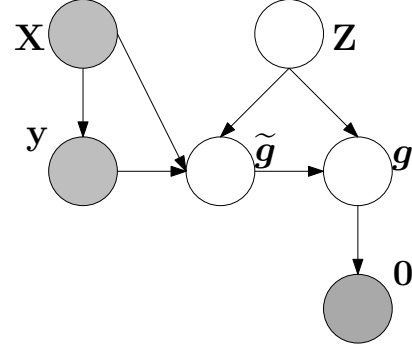


Figure 1: The graphical representation of PRGP

multivariate Gaussian distribution,

$$p(\mathbf{g}|\mathbf{Z}) = \mathcal{N}(\mathbf{g}|\mathbf{0}, \Sigma) = \mathcal{N}(\mathbf{0}|\mathbf{g}, \Sigma) \quad (5)$$

where  $\mathbf{g} = [g(\mathbf{z}_1), \dots, g(\mathbf{z}_m)]^\top$ ,  $[\Sigma]_{ij} = \kappa(\mathbf{z}_i, \mathbf{z}_j)$  and  $\kappa(\cdot, \cdot)$  is another kernel. We can see that placing a finite GP prior over  $g$  is equivalent to sampling a set of virtual observations  $\mathbf{0}$ , due to the symmetry of the Gaussian distribution. Hence, the sampling of the inputs  $\mathbf{Z}$  and virtual observations  $\mathbf{0}$  constitute the generative component, and the probability is given by

$$p(\mathbf{0}, \mathbf{Z}|\mathbf{g}) = p(\mathbf{Z})p(\mathbf{0}|\mathbf{Z}, \mathbf{g}) = p(\mathbf{Z})\mathcal{N}(\mathbf{0}|\mathbf{g}, \Sigma). \quad (6)$$

Now, we link the conditional model (*i.e.*, standard GP) and generative model (6) via the differential equation (4). Specifically, we observe that from the GP posterior distribution (2), the posterior function of any input takes the following form,  $f(\cdot) = \mu(\cdot) + \epsilon\sqrt{v(\cdot)}$ , where  $\epsilon \sim \mathcal{N}(\epsilon|0, 1)$ ,  $\mu(\cdot)$  and  $\sqrt{v(\cdot)}$  are posterior mean and standard deviation functions. While this is a random function (due to  $\epsilon$ ), we can still apply the differentiation operator to obtain the differentiated posterior function,

$$\psi f(\cdot) = \psi \mu(\cdot) + \epsilon \psi \sqrt{v(\cdot)}. \quad (7)$$

Hence, for any input  $\mathbf{x}$ , we can sample  $\psi f(\mathbf{x})$  from  $\mathcal{N}(\cdot | \psi \mu(\mathbf{x}), (\psi \sqrt{v(\mathbf{x})})^2)$ . We therefore sample  $\tilde{\mathbf{g}} = [\psi f(\mathbf{z}_1), \dots, \psi f(\mathbf{z}_m)]^\top$  from

$$p(\tilde{\mathbf{g}}|\mathbf{Z}, \mathbf{X}, \mathbf{y}) = \prod_{j=1}^m \mathcal{N}(\tilde{g}_j | \psi \mu(\mathbf{z}_j), (\psi \sqrt{v(\mathbf{z}_j)})^2),$$

where  $\tilde{g}_j = \psi f(\mathbf{z}_j)$ . Note that  $\tilde{\mathbf{g}}$  correspond to L.H.S values of the equation (4) on  $\mathbf{Z}$ . We then use a prior for  $\mathbf{g}$  conditional on  $\tilde{\mathbf{g}}$  to tie the standard GP and the generative component,

$$p(\mathbf{g}|\tilde{\mathbf{g}}) = \mathcal{N}(\mathbf{g}|\tilde{\mathbf{g}}, v\mathbf{I}). \quad (8)$$

To reflect the fact that  $\mathbf{g}$  and  $\tilde{\mathbf{g}}$  should be identical (according to (4)), we take the limit when  $v \rightarrow 0$  so that

$p(\mathbf{g}|\tilde{\mathbf{g}}) = \delta(\mathbf{g} - \tilde{\mathbf{g}})$  where  $\delta(\cdot)$  is the Dirac delta function. Finally, the joint probability is

$$\begin{aligned} p(\mathbf{y}, \mathbf{Z}, \tilde{\mathbf{g}}, \mathbf{g}, \mathbf{0}|\mathbf{X}) &= p(\mathbf{y}|\mathbf{X})p(\mathbf{Z})p(\tilde{\mathbf{g}}|\mathbf{Z}, \mathbf{X}, \mathbf{y})p(\mathbf{g}|\tilde{\mathbf{g}})p(\mathbf{0}|\mathbf{g}, \mathbf{Z}) \\ &= \mathcal{N}(\mathbf{y}|\mathbf{0}, \mathbf{K} + \tau^{-1}\mathbf{I})p(\mathbf{Z}) \\ &\cdot \prod_{j=1}^m \mathcal{N}(\tilde{g}_j|\psi\mu(\mathbf{z}_j), (\psi\sqrt{v(\mathbf{z}_j)})^2)\delta(\tilde{\mathbf{g}} - \mathbf{g})\mathcal{N}(\mathbf{0}|\mathbf{g}, \mathbf{\Sigma}). \end{aligned} \quad (9)$$

The graphical representation of PRGP is shown in Fig. 1. The generative component fulfills a GP prior of the latent function, which, combined with the differential operator, regularizes the GP modeling of the target function  $f(\cdot)$ . In this way, we incorporate the physics to guide the learning of  $f$ , without the need for specifying the form or type of the equation. The choice of  $p(\mathbf{Z})$  is flexible. If we have no knowledge about the input distribution, we can use a uniform distribution for the bounded domain, and for unbounded domains we can use a wide Gaussian distribution with zero mean or uniform distribution on a region large enough to cover our interested predictions.

## 4 Algorithm

### 4.1 Stochastic Collapsed Inference

We now present the model inference algorithm. The exact posterior of the latent random variables  $\mathbf{g}$ ,  $\tilde{\mathbf{g}}$  and  $\mathbf{Z}$  in (9) are infeasible to calculate because they are coupled in kernels and differentiation operators. While we can use variational approximations, they will introduce extra variational parameters, complicate the optimization and affect the integration of the physics knowledge. Therefore, we marginalize out all the latent variables to conduct collapsed inference to avoid approximating their complex posteriors. Specifically, we can derive that  $p(\mathbf{y}, \mathbf{0}|\mathbf{X}) = p(\mathbf{y}|\mathbf{X})p(\mathbf{0}|\mathbf{y}, \mathbf{X})$ , where

$$\begin{aligned} p(\mathbf{0}|\mathbf{y}, \mathbf{X}) &= \int p(\mathbf{Z})p(\tilde{\mathbf{g}}|\mathbf{Z}, \mathbf{X}, \mathbf{y})p(\mathbf{g}|\tilde{\mathbf{g}})p(\mathbf{0}|\mathbf{g}, \mathbf{Z})d\mathbf{g}d\tilde{\mathbf{g}}d\mathbf{Z} \\ &= \mathbb{E}_{p(\mathbf{Z})}\mathbb{E}_{p(\tilde{\mathbf{g}}|\mathbf{Z}, \mathbf{X}, \mathbf{y})} \\ &\cdot \left[ \int \delta(\tilde{\mathbf{g}} - \mathbf{g})\mathcal{N}(\mathbf{0}|\mathbf{g}, \mathbf{\Sigma})d\mathbf{g} \right] \\ &= \mathbb{E}_{p(\mathbf{Z})}\mathbb{E}_{p(\tilde{\mathbf{g}}|\mathbf{Z}, \mathbf{X}, \mathbf{y})}[\mathcal{N}(\tilde{\mathbf{g}}|\mathbf{0}, \mathbf{\Sigma})]. \end{aligned} \quad (10)$$

Further, to allow us to adjust the importance of the generative component and so the influence of the physics during training, we weight the likelihood of the generative component by a free hyper-parameter  $\gamma \geq 0$ . The weighted marginal likelihood (Warm, 1989; Hu and Zidek, 2002) is

$$p_\gamma(\mathbf{y}, \mathbf{0}|\mathbf{X}) = p(\mathbf{y}|\mathbf{X})p(\mathbf{0}|\mathbf{X}, \mathbf{y})^\gamma. \quad (11)$$

Our inference is to maximize the log weighted marginal likelihood to optimize the kernel parameters in  $k(\cdot, \cdot)$  and  $\kappa(\cdot, \cdot)$ , the inverse noise variance

$\tau$  and unknown parameters in the differential equation,  $\log p_\gamma(\mathbf{y}, \mathbf{0}|\mathbf{X}) = \log(\mathcal{N}(\mathbf{y}|\mathbf{0}, \mathbf{K} + \tau^{-1}\mathbf{I})) + \gamma \log(\mathbb{E}_{p(\mathbf{Z})}\mathbb{E}_{p(\tilde{\mathbf{g}}|\mathbf{Z}, \mathbf{X}, \mathbf{y})}[\mathcal{N}(\tilde{\mathbf{g}}|\mathbf{0}, \mathbf{\Sigma})])$ . Obviously, the log likelihood is infeasible to compute due to the intractable expectation inside the logarithm. To address this problem, we use Jensen's equality on the log function to obtain a model evidence lower bound (ELBO),  $\log p_\gamma(\mathbf{y}, \mathbf{0}|\mathbf{X}) \geq \mathcal{L}$ , where

$$\begin{aligned} \mathcal{L} &= \log(\mathcal{N}(\mathbf{y}|\mathbf{0}, \mathbf{K} + \tau^{-1}\mathbf{I})) \\ &+ \gamma \cdot \mathbb{E}_{p(\mathbf{Z})}\mathbb{E}_{p(\tilde{\mathbf{g}}|\mathbf{Z}, \mathbf{X}, \mathbf{y})}[\log(\mathcal{N}(\tilde{\mathbf{g}}|\mathbf{0}, \mathbf{\Sigma}))]. \end{aligned} \quad (12)$$

The ELBO is still intractable, because the expectation term is not analytical. However, since the expectation is outside the logarithm, we can maximize  $\mathcal{L}$  via stochastic optimization. Specifically, each time, we first sample input locations  $\mathbf{Z}$  from  $p(\mathbf{Z})$  and then generate a parameterized sample of  $\tilde{\mathbf{g}}$ . This can be efficiently done by the reparameterization trick (Kingma and Welling, 2013): according to (7), given each sample  $\mathbf{z}_j$ , to generate a parameterized sample for  $[\tilde{\mathbf{g}}]_j = \psi f(\mathbf{z}_j)$ , we can sample a standard Gaussian random variable  $\epsilon \sim \mathcal{N}(0, 1)$ , and construct the sample by  $h_j = \psi\mu(\mathbf{z}_j) + \epsilon \cdot \psi\sqrt{v(\mathbf{z}_j)}$ . We then substitute the parameterized samples  $[h_1, \dots, h_m]^\top$  for  $\tilde{\mathbf{g}}$  in  $\log(\mathcal{N}(\tilde{\mathbf{g}}|\mathbf{0}, \mathbf{\Sigma}))$  to obtain the unbiased estimate  $\tilde{\mathcal{L}}$ . We calculate  $\nabla\tilde{\mathcal{L}}$  as an unbiased stochastic gradient of  $\mathcal{L}$ , with which we can use any stochastic optimization to estimate the model parameters.

Despite its simplicity, the ELBO  $\mathcal{L}$  in (12) includes an interesting term,  $\mathbb{E}_{p(\mathbf{Z})}\mathbb{E}_{p(\tilde{\mathbf{g}}|\mathbf{Z}, \mathbf{X}, \mathbf{y})}[\log(\mathcal{N}(\tilde{\mathbf{g}}|\mathbf{0}, \mathbf{\Sigma}))]$ , in addition to the standard GP log marginal likelihood. Jointly maximizing this term in  $\mathcal{L}$  encourages that all the possible latent function values (at  $m$  locations) obtained from the GP posterior function  $f(\cdot)$  (via the differential operator  $\psi$ ) should be considered as the samples of another GP. This can be viewed as a soft constraint over the posterior function of the original GP model. Therefore, our ELBO is also a posterior regularization objective (Ganchev et al., 2010), and our inference algorithm can be viewed as estimating a standard GP model with a soft regularization on its posterior distribution.

### 4.2 Algorithm Complexity

The time complexity for the inference of our model is  $\mathcal{O}(N^3 + m^3)$ , because it involves the calculation for two GPs: one is the standard model, and the other is in the generative component. The time complexity for prediction is still  $\mathcal{O}(N^3)$ . The space complexity is  $\mathcal{O}(N^2 + m^2)$ , including the storage of the kernel matrices of the two GPs.

## 5 Discussion and Related Work

A critical difference between PRGP and LFM is that PRGP integrates the physics knowledge as a soft regularization in GP learning while LFM makes a hard encoding

in the kernel space via Green’s functions. Not only can our soft integration accommodate more complex differential equations and expressive kernels, but also it enables a flexible combination of the physics knowledge and data information by choosing the likelihood weight  $\gamma$  and number of random input locations  $m$  (when  $m \rightarrow \infty$ , PRGP achieves the hard encoding, *i.e.*,  $\psi f(\cdot) = g(\cdot)$ ). This makes PRGP particularly useful, because in real world, physical modeling often cannot guarantee a perfect match to the data generation process; there can be some mismatch/gap. In such cases, an over-rigid integration might instead restrict the model from fully capturing information in the data and hurt the performance. On the contrary, the freedom to adjust the strength and degree of the physics constraints may allow us to better synergize/utilize the information in the both sources. An excellent follow-up work (Hartikainen et al., 2012) uses the stochastic differential equation representation of the GP prior with a stationary kernel to formulate the problem as a latent state space model. While the model does not reply Green’s function as well, it is no longer a GP and does not enjoy the nonparametric learning nature. In addition, the model only applies to differential equations with one variable (*e.g.*, ODEs) and cannot exploit more complex equations, like PDEs.

It is known that applying a linear (partial) differential operator on a GP will result in another GP (Graepel, 2003). Many excellent works have been done in this direction (Graepel, 2003; Lawrence et al., 2007; Gao et al., 2008; Alvarez et al., 2009, 2013; Raissi et al., 2017). For example, Graepel (2003) uses GPs to solve the linear equation given observed noisy forces ( $u_q(\cdot)$  in (3)). He first defines the kernel for the solution function ( $f_q(\cdot)$  in (3)) with which to derive the kernel for the forces. The kernel parameters are then estimated from the noisy forces data, given which the solution can be predicted. Raissi et al. (2017) assume both the noisy forces and solutions are observed, and they jointly model these examples in one single GP with a heterogeneous block covariance matrix. Other excellent works related to GP derivatives include (Calderhead et al., 2009; Barber and Wang, 2014; Heinonen et al., 2018) *etc.* They mainly focus on estimating parameters/operators in ODEs without latent functions/forces as assumed in LFM and our work.

Posterior regularization is a powerful inference methodology (Ganchev et al., 2010). In general, the objective includes the model likelihood on data and a penalty term that encodes the constrains over the posterior of the latent variables. Many successful posterior regularization algorithms have been proposed, *e.g.*, (He et al., 2013; Ganchev and Das, 2013; Zhu et al., 2014; Bilen et al., 2014; Libbrecht et al., 2015; Song et al., 2016). While our inference algorithm is developed for a Bayesian hy-

brid model, the ELBO optimized in the inference is a typical posterior regularization objective that estimates a standard GP model and meanwhile penalizes the posterior of the (target) function to encourage the consistency with the differential equations. This aligns with our modeling goal.

## 6 Experiments

### 6.1 Simulation

We first examined if PRGP can improve extrapolation with appropriate physics knowledge. We generated two synthetic datasets. The first dataset, *1stODE*, was simulated from a first-order Ordinary Differential Equation (ODE),  $\frac{\partial f(t)}{\partial t} + B \cdot f(t) - D = g(t)$  where  $B = D = 1$ ,  $g(t) = \sin(2\pi t) \exp(-t)$  and the initial condition  $f(0) = 0.1$ . We set the time domain  $t \in [0, 1]$ . We ran the finite difference algorithm (Mitchell and Griffiths, 1980) to obtain the accurate solution. We chose 1,001 equally spaced time points ( $t_0 = 0, t_{1000} = 1$ ) and their solution values as the dataset. The second dataset, *1dDiffusion*, was simulated from a diffusion equation with one dimensional spatial domain,  $\frac{\partial f(x,t)}{\partial t} - \alpha \frac{\partial^2 f(x,t)}{\partial x^2} = g(x,t)$  where  $\alpha = 10$ ,  $g(x,t) = 0$  and the initial condition  $f(x,0)$  is a square wave. We set the domain  $(x,t) \in [0,1] \times [0,1]$ . We ran a numerical solver to obtain the accurate solution. Then we discretized the entire spatial and time domain into a  $48 \times 101$  grid with equal spacing in each dimension. We retrieved the grid points and their solution values as our dataset.

**Competing methods.** We compared with GP regression using (1) SE-ARD kernel (GP-ARD) and (2) the deep kernel (GP-DEEP), and (3) LFM, which uses SE-ARD for the latent force (function), and then convolves it with Green’s function to obtain the kernel for the target function. To construct a deep kernel, we followed (Wilson et al., 2016) to feed the input variables to a (deep) neural network (NN) and calculated the RBF kernel over the neural network outputs. Across our experiments, we used a 5-layer NN, with 20 nodes in each hidden and output layer. We used  $\tanh(\cdot)$  as the activation function. For our method PRGP, we used the same deep kernel for the solution function. As in LFM, we used SE-ARD kernel for the latent function. We set the number of virtual observations  $m = 10$  for the generative component, and uniformly sampled the input locations from the entire domain (see (12)). We chose the weight of the generative component  $\gamma$  from  $\{0.01, 0.05, 0.1, 0.5, 1, 2, 5, 10\}$ . For both LFM and PRGP, the parameters of differential equations are unknown. All the methods were implemented with TensorFlow (Abadi et al., 2016). For our method, we used ADAM (Kingma and Ba, 2014) for stochastic inference. We ran 10K epochs to ensure convergence. For the other methods, we used L-BFGS for optimization and set the maximum number of iterations to 5K.

To test extrapolation on *1stODE*, we used the first 101 samples ( $t_i \in [0, 0.1]$ ) for training, and the remaining 900 samples ( $t_i \in (0.1, 1]$ ) for test. We show the posterior distribution of the functions learned by all the methods and the ground-truth in Fig. 2. We can see that the predictions of GPR-ARD and GPR-DEEP are largely biased when the test points are far from the training region  $[0, 0.1]$ . On average, GPR-DEEP obtains better accuracy than GPR-ARD. The root-mean-square errors (RMSEs) are {GPR-DEEP:0.21, GPR-ARD:0.25}. As a comparison, the posterior means of LFM and PRGP are much closer to the ground-truth in the test region, and the RMSEs are {LFM: 0.09, PRGP: 0.04}, showing the benefit of the incorporated physics. However, LFM is quite unstable in extrapolation: the farther away the test area, the more fluctuating the prediction. By contrast, PRGP obtains much smoother curves that are even closer to the ground-truth, and smaller posterior variances in the test region. Hence, it shows that the LFM kernel obtained from shallow kernel convolution is less expressive/powerful than the regularized deep kernel in PRGP. Note that unlike GPR-ARD/DEEP, both LFM and PRGP estimated non-trivial posterior variances (*i.e.*, not extremely close to 0) in the training region, implying that the physics also helps prevent GPs from overfitting.

Since for diffusion equations, LFM cannot derive the kernel for time variable  $t$ , for a fair comparison on *1dDiffusion*, we fixed  $t = 0.5$  and used the 48 spatial points as the training inputs. While the kernel of LFM is for the spatial input only, all the other methods used both the spatial and time inputs. We then evaluated the posterior distribution of the function values at all the grid points ( $48 \times 101$ ) in the entire domain. We report the absolute difference between the posterior mean and ground-truth in Fig. 3a-d. From Fig. 3a and b, we can see that the prediction errors of GPR-ARD/DEEP are close to 0 (dark colors) in regions close to the training data ( $t = 0.5$ ). However, when the test points are getting far away, say, close to the boundary ( $t = 0$  or  $1$ ), the error grows significantly (see the bright colors). Overall, GPR-DEEP achieves smaller extrapolation error than GPR-ARD, implying an advantage of using more flexible kernels. From Fig. 3c, we can see that while LFM misses the time information, it still exhibits better extrapolation results, as compared with GPR-ARD/DEEP. It shows the benefit of the physics knowledge. Finally, PRGP achieves even smaller prediction error (*i.e.*, darker) when  $t$  is away from the training time point and exhibits even best extrapolation performance. The RMSEs of all the methods are {GPR-ARD: 0.18, GPR-DEEP: 0.11, LFM: 0.09, PRGP:0.07}. We also examined the predictive standard deviation of each method. It shows that PRGP also reduces the uncertainty of the extrapolation prediction. The details are provided

in the supplementary material.

## 6.2 Real-World Applications

**Metal Pollution in Swiss Jura.** Next, we evaluated PRGP in real-world applications. We examined the predictive performance in terms of normalized RMSE (nRMSE) and test log-likelihood (LL). Due to the space limit, the test LL results are provided in the supplementary material (Sec. 2). We first considered predicting the metal concentration in Swiss Jura. The data were collected from 300 locations in a 14.5 km<sup>2</sup> region (<https://rdr.io/cran/gstat/man/jura.html>). The diffusion of the metal concentration is naturally modelled by a diffusion equation with the two-dimensional spatial domain,  $\frac{\partial f(x_1, x_2, t)}{\partial t} = \alpha \left( \frac{\partial^2 f(x_1, x_2, t)}{\partial x_1^2} + \frac{\partial^2 f(x_1, x_2, t)}{\partial x_2^2} \right)$ , where  $f(\cdot, \cdot, \cdot)$  is the concentration of the metal at a particular location and time point. However, the dataset do not include the time  $t_s$  when these concentrations were measured. LFM considers the initial condition  $f(x_1, x_2, 0)$  as the latent function and obtains a kernel of the locations where  $t_s$  can be viewed as a kernel parameter learned from data. In our approach, we estimated the solution function at  $t_s$ ,  $h(x_1, x_2) = f(x_1, x_2, t_s)$ . Hence, the equation can be viewed as  $\frac{\partial h^2(x_1, x_2)}{\partial x_1^2} + \frac{\partial h^2(x_1, x_2)}{\partial x_2^2} = g(x_1, x_2)$ , where the latent function  $g(x_1, x_2) = \frac{1}{\alpha} \frac{\partial f(x_1, x_2, t)}{\partial t} \Big|_{t=t_s}$ . We were interested in predicting the concentration of cadmium and copper. The input variables include the coordinates of the location  $(x_1, x_2)$ , the concentrations of {nickel, zinc} for cadmium, and {lead, nickel, zinc} for copper. For PRGP, we selected  $m$  from {10, 50, 100, 200, 500} for the generative component and  $\gamma$  from {0.01, 0.05, 0.1, 0.5, 1, 2, 5, 10}. We normalized/standardized the training inputs and then sampled latent inputs  $\mathbf{Z}$  from  $\mathcal{N}(\mathbf{0}, \mathbf{I})$  in model estimation. For LFM, we varied the number of latent forces from {1, 3, 5}. We randomly selected 50 samples for training, and used the remaining 250 samples for test. We repeated the experiments for 5 times, and report the average nRMSE and its standard deviation of each method in Fig. 4a and b. As we can see, PRGP outperforms all the competing approaches for both prediction tasks. PRGP always significantly improves upon GPR-ARD and GPR-DEEP ( $p < 0.05$ ). In addition, PRGP significantly outperforms LFM in predicting Cadmium concentration (Fig. 4b). Note that LFM does improve upon GPR-ARD in predicting Copper concentration (Fig. 4a), but not as significant as PRGP.

**Motion Capture.** We then looked into predicting trajectories of joints in the motion capture application. To this end, we used CMU motion capture database (<http://mocap.cs.cmu.edu/>), from which we used the samples collected from subject 35 in the walk and jog motion lasting for 2,644 seconds. We trained all the mod-

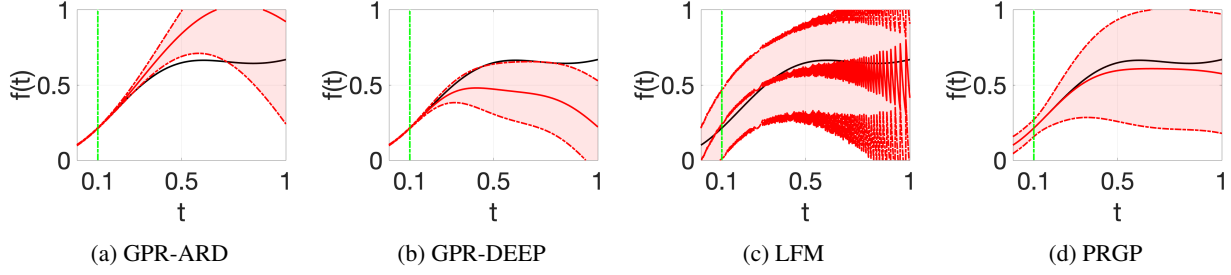


Figure 2: The posterior distribution of the learned solution functions on  $1stODE$ . The red lines in the middle are the posterior means and the red dashed lines on the boundary of the shaded region the posterior mean plus/minus one posterior standard deviation. The black line is the ground-truth solution. The training inputs stay in  $[0, 0.1]$  (left to the green line).

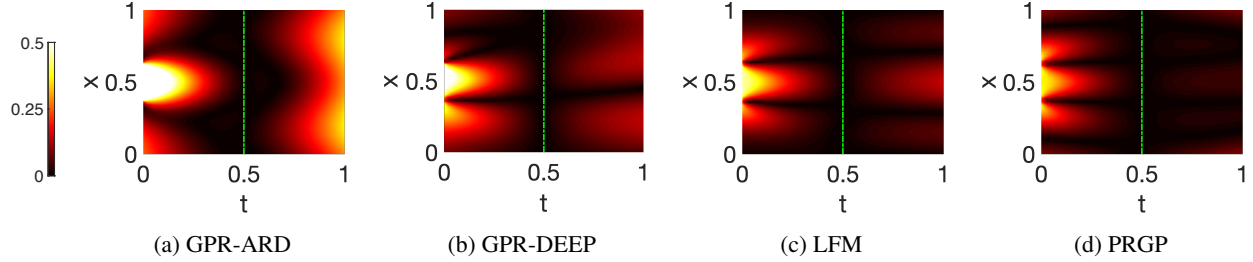


Figure 3: The absolute prediction error. The training examples stay on  $t = 0.5$  (the green line).

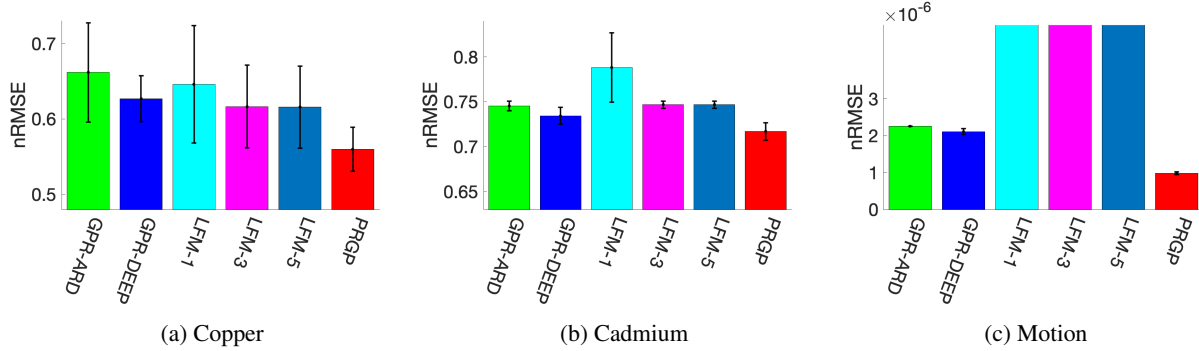


Figure 4: Metal concentration prediction in Swiss Jura (a, b) and joint angle prediction in motion capture (c). The results are averaged over 5 runs. The normalized root-mean-square error (nRMSE) in each run is computed by normalizing the RMSE by the mean of the test outputs.

els to predict the angles of Joint 60 along with time. We used the first order ODE in simulation to represent the physical model, based on which we ran LFM and PRGP. Note this physical system might be oversimplified (Alvarez et al., 2009). For LFM, we varied the number of latent forces from  $\{1, 3, 5\}$ . Again, we randomly selected 500 samples for training and 2,000 samples for test. We repeated the experiments for 5 times and report the average nRMSE and its standard deviation in Fig. 4c. As we can see, PRGP improves upon all the competing methods by a large margin. Note that LFM is even far worse than GPR-ARD. This might be because LFM over-exploits the over-simplified physics, which harms the prediction. By contrast, PRGP allows us to tune the number of virtual observations  $m$  and the likelihood weight ( $\gamma$  in (12)), and hence can consistently improve upon GPR-DEEP.

**PM2.5 in Salt Lake City.** Second, we considered predicting the Particulate Matter (PM2.5) levels across Salt

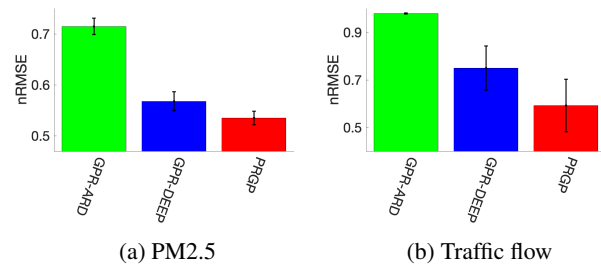


Figure 5: PM2.5 and traffic flow prediction.

Lake City. The dataset were collected from sensors' reads at different time and locations (<https://aqand.u.org/>). We chose the time range from 07/04/2018 to 07/06/2018. Following (Wang et al., 2018), we used the diffusion equation plus a source term (*i.e.*, the latent function) to represent the physical model,  $\frac{\partial f(x_1, x_2, t)}{\partial t} - \alpha \sum_{j=1}^2 \frac{\partial^2 f(x_1, x_2, t)}{\partial x_j^2} = g(x_1, x_2, t)$ , where  $f$  is the concentration level and  $g$  the source term. The input variables

include both the location coordinates and detailed time points. Since LFM cannot construct a full kernel of the input variables from the physics, we did not test it to avoid unfair comparisons. We trained GPR-ARD and GPR-DEEP with both the spatial and time inputs. We randomly selected 500 samples for training and 2,000 samples for test. We repeated the experiments for 5 times and report the average nRMSE and its standard deviation in Fig. 5a. As we can see, with a more flexible kernel, GPR-DEEP improves upon GPR-ARD significantly, and with the incorporation of the physics, PRGP in turn outperforms GPR-DEEP significantly ( $p < 0.05$ ).

**High-Way Traffic Flow Prediction.** Finally, we applied PRGP to predict the traffic flow in the interstate highway 215 across Utah state. The Utah Department of Transportation (UDOT) has installed sensors every a few miles along the high way. Each sensor counts the number of vehicles passed every minute, and sends the data back to a central database. The real time data and road conditions are available at <https://udot.iteris-pems.com/>. We used the data collected by 20 sensors continuously installed in a segment of 30 miles, and the time was chosen from 08/05/2019 to 08/11/2019. The input variables include the location coordinates of each sensor and the time of each read. Following (Nagatani, 2000), we used the Burger’s equation plus a source term to describe the system,  $\frac{\partial f}{\partial t} + f \cdot \sum_{j=1}^2 \frac{\partial f}{\partial x_j} - \nu \sum_{j=1}^2 \frac{\partial^2 f}{\partial x_j^2} = g(x_1, x_2, t)$ , where  $f$  is the traffic flow,  $\nu$  the unknown viscous coefficient, and  $g$  the source term, *i.e.*, the latent function. Note that the equation is nonlinear and we do not have an analytical form of Green’s function. Hence we cannot use LFM to incorporate the physics to enhance GP training. Hence we compared with GPR-ARD and GPR-DEEP only. We randomly selected 500 and 2,000 samples for training and test, respectively, and repeated for 5 times. The average nRMSEs and the standard deviations are reported in Fig. 5b. As we can see, GPR-DEEP significantly outperforms GPR-ARD, which demonstrates the advantage of the more expressive, deep kernel. More important, PRGP further improves upon GPR-DEEP, showing that the physics incorporated by our approach indeed promotes the predictive performance.

## 7 Conclusion

We have presented PRGP, a physics regularized GP model that can flexibly incorporate physics knowledge from incomplete linear/nonlinear differential equations to promote GP training for limited data and extrapolation. In the future work, we will extend our model with sparse GP approximations (Hensman et al., 2013) and explore the effect of physics for large-scale applications.

## Broader Impact

This work can be used in a variety prediction and engineering development tasks. Therefore, the work has potential positive impacts in the society if it is used to forecast weather and air quality, develop safe and high-capacity batteries, traffic management, and all the other tasks that can benefit human lives. At the same time, this work may have some negative consequences if it is used to study weapon effects or develop new weapons.

## References

- Abadi, M., Barham, P., Chen, J., Chen, Z., Davis, A., Dean, J., Devin, M., Ghemawat, S., Irving, G., Isard, M., et al. (2016). Tensorflow: A system for large-scale machine learning. In 12th USENIX Symposium on Operating Systems Design and Implementation (OSDI 16), pages 265–283.
- Alvarez, M., Luengo, D., and Lawrence, N. D. (2009). Latent force models. In Artificial Intelligence and Statistics, pages 9–16.
- Alvarez, M. A., Luengo, D., and Lawrence, N. D. (2013). Linear latent force models using Gaussian processes. IEEE transactions on pattern analysis and machine intelligence, 35(11):2693–2705.
- Arfken, G. B., Weber, H. J., and Harris, F. E. (2011). Mathematical Methods for Physicists: A Comprehensive Guide. Academic Press.
- Barber, D. and Wang, Y. (2014). Gaussian processes for bayesian estimation in ordinary differential equations. In International Conference on Machine Learning, pages 1485–1493.
- Bilen, H., Pedersoli, M., and Tuytelaars, T. (2014). Weakly supervised object detection with posterior regularization. In British Machine Vision Conference, volume 3.
- Calderhead, B., Girolami, M., and Lawrence, N. D. (2009). Accelerating bayesian inference over nonlinear differential equations with gaussian processes. In Advances in neural information processing systems, pages 217–224.
- Courant, R. and Hilbert, D. (2008). Methods of Mathematical Physics: Partial Differential Equations. John Wiley & Sons.
- Ganchev, K. and Das, D. (2013). Cross-lingual discriminative learning of sequence models with posterior regularization. In Proceedings of the 2013 Conference on Empirical Methods in Natural Language Processing, pages 1996–2006.
- Ganchev, K., Gillenwater, J., Taskar, B., et al. (2010). Posterior regularization for structured latent variable



- models. Journal of Machine Learning Research, 11(Jul):2001–2049.
- Gao, P., Honkela, A., Rattray, M., and Lawrence, N. D. (2008). Gaussian process modelling of latent chemical species: applications to inferring transcription factor activities. Bioinformatics, 24(16):i70–i75.
- Graepel, T. (2003). Solving noisy linear operator equations by gaussian processes: Application to ordinary and partial differential equations. In ICML, pages 234–241.
- Hartikainen, J., Seppänen, M., and Särkkä, S. (2012). State-space inference for non-linear latent force models with application to satellite orbit prediction.
- He, L., Gillenwater, J., and Taskar, B. (2013). Graph-based posterior regularization for semi-supervised structured prediction. In Proceedings of the Seventeenth Conference on Computational Natural Language Learning, pages 38–46.
- Heinonen, M., Yildiz, C., Mannerström, H., Intosalmi, J., and Lähdesmäki, H. (2018). Learning unknown ode models with gaussian processes. In International Conference on Machine Learning, pages 1959–1968.
- Hensman, J., Fusi, N., and Lawrence, N. D. (2013). Gaussian processes for big data. In Proceedings of the Conference on Uncertainty in Artificial Intelligence (UAI).
- Hu, F. and Zidek, J. V. (2002). The weighted likelihood. Canadian Journal of Statistics, 30(3):347–371.
- Kingma, D. P. and Ba, J. (2014). Adam: A method for stochastic optimization. arXiv preprint arXiv:1412.6980.
- Kingma, D. P. and Welling, M. (2013). Auto-encoding variational bayes. arXiv preprint arXiv:1312.6114.
- Lapidus, L. and Pinder, G. F. (2011). Numerical solution of partial differential equations in science and engineering. John Wiley & Sons.
- Lasserre, J. A., Bishop, C. M., and Minka, T. P. (2006). Principled hybrids of generative and discriminative models. In 2006 IEEE Computer Society Conference on Computer Vision and Pattern Recognition (CVPR’06), volume 1, pages 87–94. IEEE.
- Lawrence, N. D., Sanguinetti, G., and Rattray, M. (2007). Modelling transcriptional regulation using gaussian processes. In Advances in Neural Information Processing Systems, pages 785–792.
- Libbrecht, M. W., Hoffman, M. M., Bilmes, J. A., and Noble, W. S. (2015). Entropic graph-based posterior regularization: Extended version. In Proceedings of the International Conference on Machine Learning.
- Mitchell, A. R. and Griffiths, D. F. (1980). The finite difference method in partial differential equations. Number BOOK. John Wiley.
- Nagatani, T. (2000). Density waves in traffic flow. Physical Review E, 61(4):3564.
- Olsen-Kettle, L. (2011). Numerical solution of partial differential equations. Lecture notes at University of Queensland, Australia.
- Polyanin, A. D. and Nazaikinskii, V. E. (2015). Handbook of linear partial differential equations for engineers and scientists. Chapman and hall/crc.
- Raissi, M., Perdikaris, P., and Karniadakis, G. E. (2017). Machine learning of linear differential equations using gaussian processes. Journal of Computational Physics, 348:683–693.
- Song, Y., Zhu, J., and Ren, Y. (2016). Kernel bayesian inference with posterior regularization. In Advances in Neural Information Processing Systems, pages 4763–4771.
- Wang, Y., Wang, H., Chang, S., and Avram, A. (2018). Prediction of daily pm<sub>2.5</sub> concentration in china using partial differential equations. PloS one, 13(6):e0197666.
- Warm, T. A. (1989). Weighted likelihood estimation of ability in item response theory. Psychometrika, 54(3):427–450.
- Wilson, A. G., Hu, Z., Salakhutdinov, R., and Xing, E. P. (2016). Deep kernel learning. In Artificial Intelligence and Statistics, pages 370–378.
- Zhu, J., Chen, N., and Xing, E. P. (2014). Bayesian inference with posterior regularization and applications to infinite latent svms. The Journal of Machine Learning Research, 15(1):1799–1847.

## Supplementary Materials

### 8 Posterior Standard Deviation

On the *1dDiffusion* dataset (see Section 6.1 of the main paper), we also examined the posterior standard deviations of all the methods, as shown in Fig. 6. We can see that the posterior standard deviations (PSDs) of GPR-ARD/DEEP are both close to 0 in the training region, and quickly grow when the inputs move away. On average GPR-DEEP shows smaller PSDs and smoother changes. By contrast, LFM and PRGP obtain PSDs quite uniformly across the entire domain and less than GRP-ARD/DEEP. It means that the physics knowledge help inhibit overfitting and reduce the uncertainty in extrapolation. Compared with LFM, PRGP obtains even smaller PSDs (darker color) across the domain, showing even smaller uncertainty in

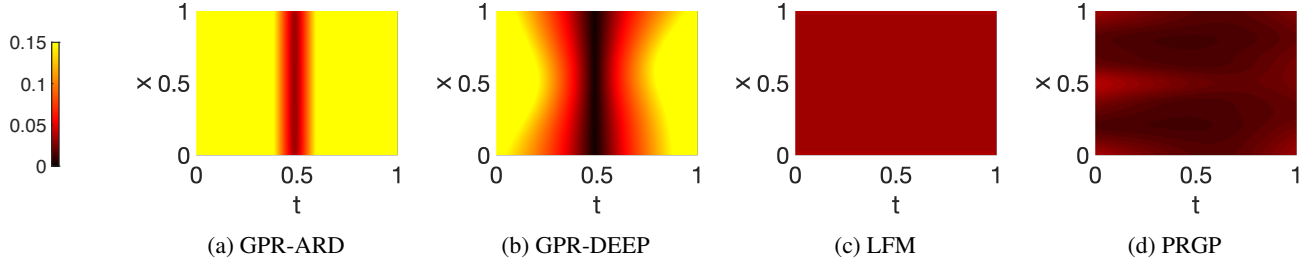


Figure 6: The posterior standard deviation on *IdDiffusion*.

extrapolation. This is consistent with the results on the *IstODE* dataset.

## 9 Test Log-likelihood on Real-World Datasets

In Fig. 7 and 8, we report the test log-likelihood (LL) of all the methods in the real-world applications in Section 6.2 of the main paper. Note that since test LLs are negative (smaller than zero) in most datasets, the corresponding bar plots are shown inverted for a convenient comparison. As we can see, our method (PRGP) consistently outperforms all the competing methods, and in many cases by a large margin. GPR-DEEP always obtains test LLs larger than or comparable to GPR-ARD except that in Fig. 8 a, GPR-DEEP is lightly worse. It demonstrates the advantage of more expressive kernels. PRGP further improves upon GPR-DEEP in all the cases, showing that the physics knowledge are effectively exploited and indeed help with the prediction. Especially, in Fig. 8a, while GPR-DEEP obtains slightly smaller test LLs than GPR-ARD, after PRGP regularizes the same deep kernel with physics, the test LLs are greatly improved. Note that, similar to nRMSE results, we can see LFM improves upon GPR-ARD in some cases, *e.g.*, LFM-3 in Fig. 7 a and b, but in other cases are even worse, *e.g.*, in Fig. 7 c. This might be because the rigid incorporation (hard-coding) of the physics in LFM might even hurt the performance when there is a significant mismatch to the actual data. For example, a first-order ODE might be too simple to describe the motion data in Fig. 7 c. Overall, the test LL results are consistent with nRMSEs shown in the main paper.

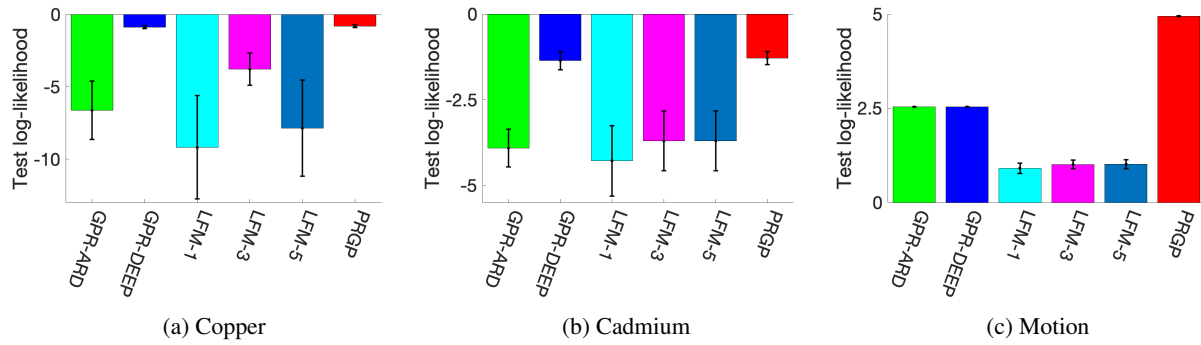


Figure 7: Test log-likelihood (LL) in Swiss Jura (a, b) and joint angle prediction in motion capture (c). The results are averaged over 5 runs.

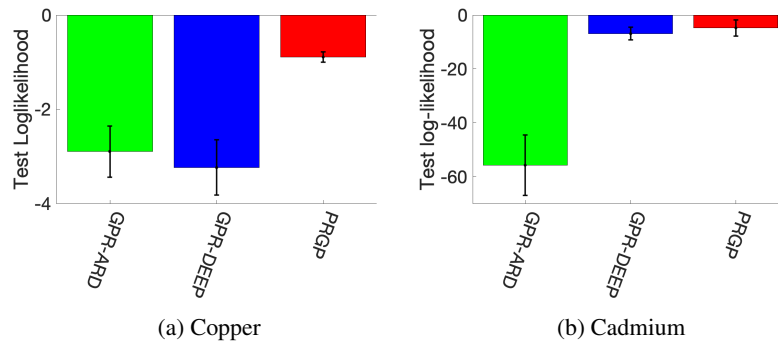


Figure 8: Test log-likelihood (LL) for PM2.5 and traffic flow datasets. The results are averaged over 5 runs.